Strain rate effects in phenolic composites and phenolic-impregnated honeycomb structures

Sebastian Heimbs [a,*], Sebastian Schmeer [b], Peter Middendorf [a], Martin Maier [b]

[a] *EADS Innovation Works, Structures Engineering, Production and Mechatronics Department, 21129 Hamburg, Germany*
[b] *Institute for Composite Materials (IVW), Kaiserslautern University of Technology, 67663 Kaiserslautern, Germany*

Abstract

The influence of the loading rate on the material behaviour of glass fibre reinforced phenolic composites and phenolic resin-impregnated aramid paper (Nomex®) honeycomb structures was investigated experimentally. The composite specimens were made of woven fabric plies and loaded in tension and shear. Two types of Nomex® honeycomb specimens (hexagonal and over-expanded) were loaded in uniaxial compression in all three material directions. Quasi-static test results were compared to dynamic test data obtained on a drop tower, where different strain rates from 10 s^{-1} to 300 s^{-1} were tested. The glass/phenolic composite material showed a remarkable strain rate effect at higher loading rates with over 80% increase in tensile strength. Also for the Nomex® honeycomb an increase of the stress level of up to 30% was observed. These material characteristics should be taken into account in case of dynamic analysis (e.g. crash, impact) of honeycomb sandwich panels for public transport applications, which are usually made from these phenolic materials.
© 2007 Elsevier Ltd. All rights reserved.

Keywords: A. Structural materials; B. Impact behaviour; B. Mechanical properties; B. Stress/strain-curves; Honeycomb

1. Introduction

Fibre reinforced composites are characterised by high weight-specific stiffness and strength properties and are therefore preferred lightweight materials for the maritime, railway and aeronautical transportation industries. An even higher stiffness-to-weight ratio may be achieved by employing the sandwich construction principle: Separating two thin composite facesheets by a cellular core results in considerably higher bending stiffness compared to a monolithic structure of the same weight. Such lightweight sandwich structures are generally used for interior panels in ground and air transportation applications, where the requests for weight saving are as important as fire safety properties for occupant safety. For this reason phenolic resin-based glass fibre reinforced plastics (GFRP) or carbon fibre reinforced plastics (CFRP) are typically used as facesheet material. The core structure commonly consists of a phenolic resin-impregnated aramid paper honeycomb structure which is commercially known as Nomex® honeycomb. Phenolic resins are polycondensation products of phenol and formaldehyde and, in contrast to other resin types, characterised by outstanding fire safety properties like low smoke emission, low toxicity and low heat release [1–4].

Although phenolic resins were among the first polymers developed and have been commercially available for about a hundred years, nowadays they have become an almost exotic material, which is primarily due to delicate processing, the emission of volatile products during hardening and comparably low mechanical properties like interlaminar shear strength or sandwich peel strength. The majority of resins used for composite materials are epoxy, polyester and vinylester resins. Accordingly, most scientific papers cover the latter types of resins. Only few publications contain information about mechanics or material characteristics of phenolic composites [5–12].

---

* Corresponding author. Tel.: +49 40 743 84257; fax: +49 40 743 81517.
E-mail address: sebastian.heimbs@eads.net (S. Heimbs).

When designing sandwich panels for short-time dynamic loads, which can occur in transportation applications by high decelerations or impact, it is necessary to have information about the influence of loading rate on the material properties of both facesheet and core. It is well known that in case of high loading rates an increase in material stiffness and strength compared to the static behaviour may occur, which is referred to as the strain rate effect. When this effect is neglected, dynamic finite element (FE) simulation results based on static material data often do not agree with experimental results, or constructions are too conservative in design, inhibiting potential weight savings.

So far the strain rate effect of honeycomb structures has been primarily investigated for aluminium honeycomb. While in [13] no effect was observed during dynamic flatwise compression testing (Charpy impact test, strain rate $100 \, s^{-1}$), a 10% increase of crush strength compared to static values was reported in [14] (drop weight test, $200 \, s^{-1}$), a 15% increase in [15] (drop weight test), a 20% increase in [16–18] (drop weight test, $40 \, s^{-1}$), a 33% increase in [19] (gas gun test, $1000 \, s^{-1}$), a 40% increase in [20] (split Hopkinson pressure bar, $800 \, s^{-1}$) and a 50% increase in [21–23] (gas gun test, $2000 \, s^{-1}$).

The strain rate effect of Nomex® honeycomb was investigated in [22,23]. Here flatwise compression tests were conducted under high loading rates (gas gun test) and a 10% increase in crush strength compared to static tests was reported. Also in [24] a slight increase was observed, although dynamic testing was conducted only in the medium strain rate domain of $5 \, s^{-1}$.

For material modelling of honeycomb structures, as for crash or impact simulations using commercial dynamic FE-codes, the nonlinear compressive stress–strain-relationship up to full compaction has to be defined not only in thickness direction but generally in all three material directions [25]. In [26] the in-plane deformation behaviour of aluminium honeycomb is investigated analytically and phenomenologically. In-plane compression tests with regard to strain rate effects were conducted on aluminium honeycomb specimens in [27] (drop weight test, strain rate $66 \, s^{-1}$, 30% increase), [28] (strain rate $100 \, s^{-1}$) and [29] (drop weight test, strain rate $500 \, s^{-1}$). Dynamic in-plane compression testing on polycarbonate honeycomb is reported in [30], where an increase in crush strength was also observed. Dynamic in-plane compression testing of Nomex® honeycomb has to the authors' best knowledge not been reported before. Usually arbitrary assumptions are made concerning the in-plane structural behaviour due to nonexisting material data [31].

The aim of this paper is to fill the gap in lacking knowledge of the strain rate effect on the material properties of phenolic GFRP composites and phenolic resin-impregnated aramid paper honeycomb in all material directions. Therefore, results of dynamic tests on a drop tower facility are compared to static reference test data. The tensile and shear behaviour of GFRP composites as well as the in-plane and out-of-plane compressive behaviour of two types of Nomex® honeycomb are investigated.

2. Specimens

2.1. GFRP specimens

The GFRP specimens were made of satin-weave fabric E-glass fibre reinforced phenolic resin prepregs of the type Stesalit PHG 600-68-50 with a cured ply thickness of 0.33 mm. Two different GFRP plates were manufactured: One plate consisted of six equally oriented plies for the determination of the tensile behaviour in warp and weft direction, respectively, and one plate was made from eight plies in a symmetric ± 45°-configuration for the determination of the shear properties. Both plates were manufactured on a hot press at a temperature of 135 °C, a pressure of 2.0 bar and a curing cycle time of 90 min. Specimens were machined on a precision saw and equipped with GFRP doubler tabs on both sides. For each test series at least five specimens were tested. Tensile behaviour was determined for both warp and weft direction of the fabric prepregs.

Fig. 1 shows a microscopic view of a cross-section of a 6-ply specimen. A large void content is clearly visible, which is the result of the polycondensation reaction of the phenolic resin. Water is the concurrent loss causing internal pressure and voids in the phenolic matrix and the surface of the composite. This is characteristic for phenolic resins and does not occur in epoxy resins, which are a product of polyaddition reactions.
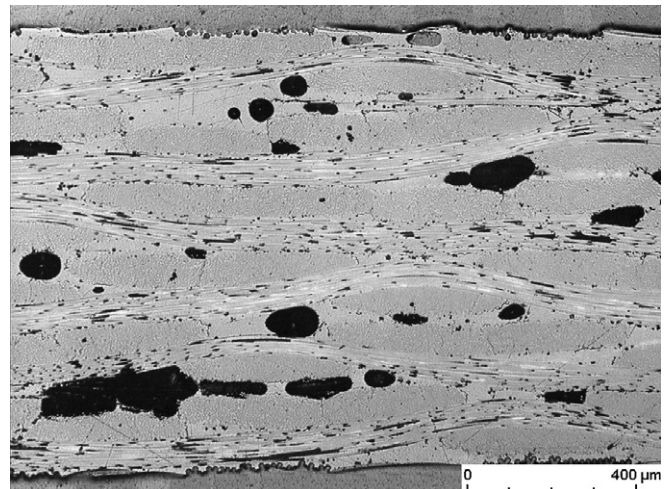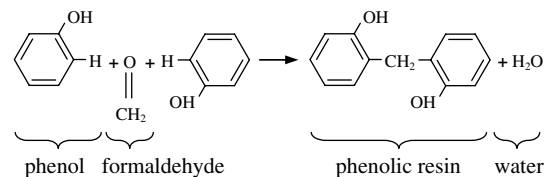

Fig. 1. Cross-section of 6-ply woven fabric GFRP specimen.

A fibre volume fraction of 48% was determined by the SEM-photomicrographic technique and resin burn-off method according to ASTM D2584.

2.2. Honeycomb specimens

Two different types of aerospace grade low density Nomex® honeycomb were investigated in this study: a hexagonal and an over-expanded structure from the manufacturer Schütz Cormaster. These honeycombs are manufactured in an expansion process, in which sheets of Nomex® paper are equipped with adhesive strips and stacked with a shift. This block of Nomex® paper sheets is then expanded to a hexagonal cell geometry and finally dipped in phenolic resin several times until the specific density is achieved. The over-expanded cell configuration is obtained by expanding the hexagonal cell until it forms a rectangle. It is bendable in the L-direction and used as sandwich core material for curved surfaces. Cell sizes and densities of both types of honeycomb are listed in Table 1.

All specimens were cut out of large honeycomb plates with a thickness of 14.6 mm. The specimens for in-plane compression tests had a size of 200 mm × 50 mm (Fig. 2),

Table 1
Honeycomb types investigated in this study

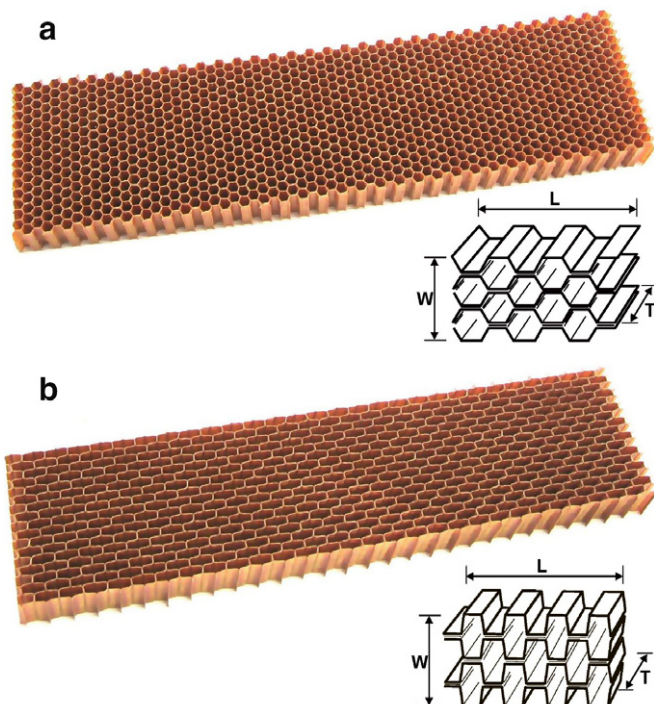| Cell configuration	Cell size (mm)	Density (kg/m³)	Type
Hexagonal	3.2	48	Cl-3.2-48
Over-expanded	4.8	48	Cl-4.8-48ox

Fig. 2. Nomex® honeycomb specimens for in-plane compression tests: (a) hexagonal; (b) over-expanded cell configuration.

for out-of-plane compression tests 50 mm × 50 mm. The latter tests were performed as 'bare compression' and 'stabilised compression' with GFRP facesheets glued to both sides of the specimens. The honeycomb in-plane material directions are illustrated in Fig. 2 and referred to as the L-direction (ribbon direction), W-direction (direction perpendicular to the ribbon), and the out-of-plane direction as the T-direction (thickness direction). In this illustration it can also be seen that the cell walls oriented in the L-direction are twice as thick (=double cell walls) as the other cell walls (=single cell walls), which is a result of gluing the paper sheets in the manufacturing process.

3. Experimental setup

3.1. Static testing

Static testing of GFRP and honeycomb specimens was conducted on an Instron universal testing facility with a cross-head speed of 1 mm/min resulting in strain rates of 10^{-4}–10^{-3} s^{-1}. Tensile tests on GFRP specimens were conducted according to DIN EN ISO 527-4. Two perpendicular strain gauges were used to measure the longitudinal and transverse deformation of the specimen. Shear behaviour was determined according to DIN EN 6031 using ±45°-tensile specimens equipped with strain gauges parallel and transverse to the loading direction.

For the honeycomb compression tests according to DIN 53291 the cross-head displacement and force data were recorded in order to obtain force–displacement-curves and convert them into engineering stress–strain-curves. In addition to static testing the maximum cross-head speed of 300 mm/min of the Instron testing apparatus was used in order to conduct compression tests in the low strain rate domain of 0.1–0.5 s^{-1}. Compression testing was conducted in L-, W- and T-direction.

3.2. Dynamic testing

A drop weight tower was used for dynamic testing at higher loading rates (10–300 s^{-1}) for both GFRP and honeycomb specimens. While for the honeycomb compression tests the specimens were placed on an aluminium block connected to the load cell, a special apparatus was used for the GFRP tensile tests, in which the specimens were mounted vertically. The falling mass impacted the mounting device on the lower end of the specimen inducing a tensile load, while the upper end of the specimen was connected to the load cell (Fig. 3).

A laser distance measurement system was used for displacement recording. For the GFRP specimens the use of strain gauges was impracticable at these loading rates, so an optical measurement of the longitudinal and transverse material deformation was incorporated: The specimens were marked with a high contrast colour grid, which was recorded with a VDS Vosskühler HCC-1000F high speed camera with a frame rate of 6832 fps during the dynamic
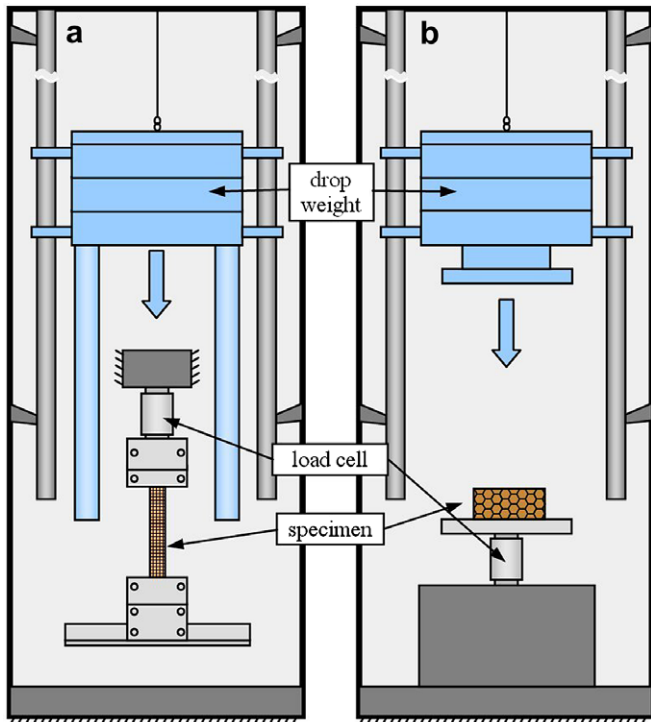
Fig. 3. Drop weight test apparatus for (a) tensile tests of GFRP specimens, (b) compression tests of honeycomb specimens.
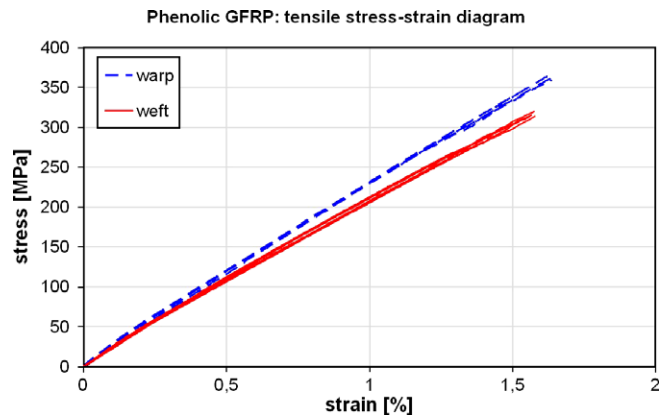

Fig. 4. GFRP tensile test results: static stress–strain-curves for warp and weft direction.

Table 2
Static Young's modulus of phenolic GFRP in warp and weft direction

Mat. direction	Stiffness (MPa)	Standard deviation (MPa)	Increase (%)
Weft	23043	331	–
Warp	24745	208	7.4

Table 3
Static tensile strength of phenolic GFRP in warp and weft direction

Mat. direction	Strength (MPa)	Standard deviation (MPa)	Increase (%)
Weft	325	9.0	–
Warp	352	18.3	8.3

test. The material deformation could be obtained by analysing these high speed films and measuring the relative displacement of specific pixels.

For both GFRP and honeycomb specimens two different strain rates were tested on the drop tower facility. The lower one was limited by the lowest possible drop height (in combination with the maximum possible mass in order to provide enough kinetic energy to destroy the specimen), the higher one was limited by the highest possible drop height (in combination with the minimum possible mass). The GFRP specimens were dynamically tested at strain rates of $10\ s^{-1}$ and $50\ s^{-1}$, the honeycomb specimens at strain rates of $10\ s^{-1}$ and $50\ s^{-1}$ (in-plane) as well as $150\ s^{-1}$ and $300\ s^{-1}$ (out-of-plane).

SAE 300 and SAE 500 filters were used in order to filter out superposed high frequency oscillations. This was conducted to increase comparability of dynamic and static test data, although structure's oscillations are always associated with dynamic loads and particularly with impacts and they cannot be denoted as noise [32].

4. Results and discussion

4.1. GFRP specimens

Static tensile testing of GFRP specimens was conducted in warp and weft direction to analyse the difference between the material directions of the woven fabric prepregs. The resulting stress–strain-curves of five specimens in each case (Fig. 4) are highly reproducible and show

8% higher stiffness (Table 2) and strength values (Table 3) for the warp direction. This is primarily due to the higher yarn density of 22 yarns per cm in warp direction compared to 21 yarns per cm in weft direction. In this case the Young's modulus was calculated as the slope of the strain interval from 0.05% to 0.25% according to the test standard.

In practice, for most constructions the fabric orientation is not specified and based on manufacturing criteria, design calculations are often carried out conservatively using the lower weft direction values. For this reason dynamic testing was primarily conducted in weft direction. The tensile stress–strain relationship for three different strain rates in weft direction is illustrated in Fig. 5. A remarkable increase of tensile strength is visible for higher loading rates. For a strain rate of $50\ s^{-1}$ the averaged increase is 88% compared to the static value (Table 4). The relationship between strain rate and strength increase is illustrated in a strain rate diagram on a logarithmic scale (Fig. 6). Even if no data for the medium strain rate domain is available, the typical curve with a distinctive plateau without strength increase for lower strain rates and a steep slope for higher strain rates can be plotted. The higher values for the warp direction compared to the weft direction are also visible in this diagram. The domain, in which a distinctive strain rate
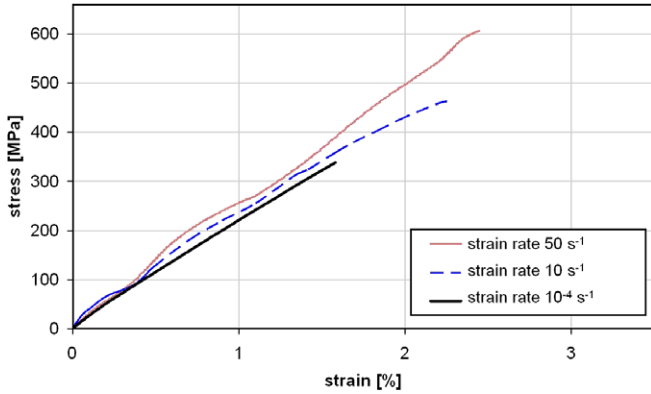
Fig. 5. GFRP tensile test results: stress–strain-curves at different strain rates (weft direction).

Table 4
Strain rate dependent increase of tensile strength for phenolic GFRP in weft direction

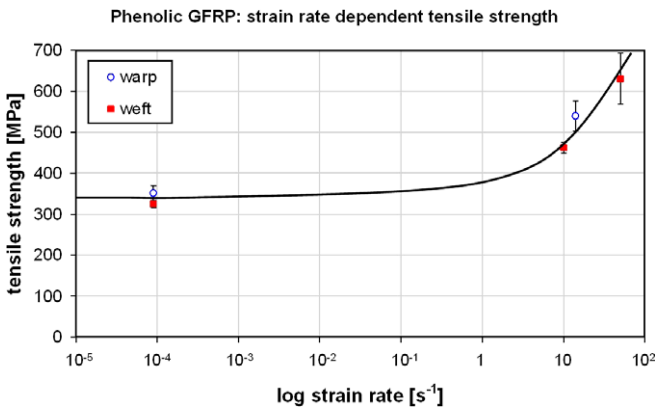| Strain rate (s^{-1})	Strength (MPa)	Standard deviation	Increase (%)
10^{-4}	325	9.0	–
10	462	13.5	42
50	610	40.7	88

Fig. 6. GFRP strain rate diagram: strain rate dependent tensile strength in warp and weft direction.

effect occurs, begins with strain rates exceeding approximately 1 s^{-1}. The failure strain increases with higher loading rates as well (Table 5). This effect is typical for glass fibre reinforced plastics, while the failure strain remains nearly constant for carbon fibre reinforced plastics and decreases for aramid fibre reinforced plastics [33–35]. The

Young's modulus also seems to increase marginally according to Fig. 5. However, because even after data filtering some residual oscillations remained in the high strain rate curves, which made the calculation of a comparable slope impracticable, this effect was not quantified.

In case of shear behaviour, higher loading rates also lead to a remarkable increase of the stress-curves (Fig. 7). However, there is only a small difference between the two higher strain rates 10 s^{-1} and 50 s^{-1}. The increase of shear strength compared to the static case is 25% and 33% respectively (Table 6). The shear modulus also increases marginally, but this phenomenon was not quantified as in the case of tensile stiffness due to oscillations in the initial slope of the stress-curves. The maximum shear strain before rupture of the specimens is nearly constant for all strain rates and does not seem to be affected by loading rate.

A generally accepted explanation for the strain rate effect of composite materials is still not available and a complex issue due to the interaction of reinforcement fibres and matrix phase. Different theories can be found in the according literature. One theory explaining the strength increase at higher loading rates is a change in failure mode with interface failure of fibre and matrix as an increasing source of damage for higher strain rates [12,36]. A second theory found in [12] is based on the influence of the elastic interaction between fibre and matrix, which means that woven fabric reinforced composites show a higher strain rate effect than unidirectional reinforced ones due to a larger interaction zone. Furthermore, in [12] it is stated that the strain rate effect of the composite material is caused
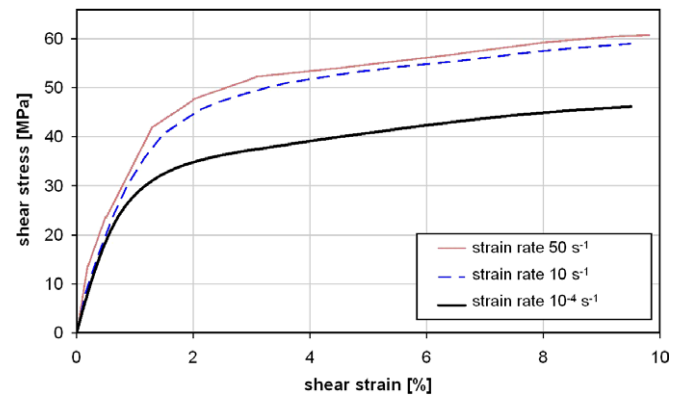

Fig. 7. GFRP ±45° tensile test results: shear stress–shear strain-curves at different strain rates.

Table 5
Strain rate dependent increase of tensile failure strain for phenolic GFRP in weft direction

Strain rate (s^{-1})	Failure strain (%)	Standard deviation (%)	Increase (%)
10^{-4}	1.62	0.09	–
10	2.38	0.16	47
50	2.48	0.11	53

Table 6
Strain rate dependent increase of shear strength for phenolic GFRP

Strain rate (s^{-1})	Shear strength (MPa)	Standard deviation (MPa)	Increase (%)
10^{-4}	45.8	1.24	–
10	57.1	2.18	25
50	61.2	0.81	33

by the viscoelasticity of the resin material, since the glass fibre sensitivity to strain rate is considered to be small or none. This is contradictory to [37], where static and dynamic tests in the strain rate domain of 10^{-4} to $1100\ \mathrm{s}^{-1}$ were conducted on pure E-glass fibre bundles and a rate dependency with an increase of strength and failure strain of almost 300% for the highest loading rates was reported. Also in [38] a considerable strain rate effect was obtained for E-glass fibre reinforced epoxy and pure E-glass fibre bundles, while pure epoxy specimens showed no strength increase for strain rates between 10^{-6} and $30\ \mathrm{s}^{-1}$. Here the rate sensitivity of the composite material is primarily ascribed to the strength increase of the fibre material. This is also presumed to be the explanation for the strain rate effect in the current investigation, which comprises a reinforcement of E-glass fibres as well. This theory is supported by the fact that the strain rate effect for shear loads is lower than for tensile loads, since the shear behaviour of composites is less fibre-dominated than the tensile behaviour (Tables 5 and 6).

4.2. Honeycomb specimens

4.2.1. Hexagonal honeycomb

Out-of-plane compression testing of hexagonal honeycomb specimens was conducted with and without facesheets (stabilised/bare compression). In case of bare compression the free ends of the honeycomb specimen have translational and rotational degrees of freedom and crushing is initiated at one of the free ends. By contrast, the stabilised compression test with facesheets represents the sandwich nature. In this case the cell wall edges are clamped and cell wall buckling and crushing occurs somewhere in the middle of the specimen. These results are much more useful for the designer [39].

Fig. 8 shows the sequence of cell wall deformation during flatwise compression loading. While Fig. 8a shows the initial configuration, in Fig. 8b a number of cell wall buckling waves are visible. Collapse of the cells occurs in the middle of the specimen due to loss of stability (Fig. 8c), where the folding process of the cell walls continues during displacement-controlled compression.

Figs. 9 and 10 show the respective stress–strain-diagrams. All of these and the following curves represent the mean data of five tests with very similar curves of the respective specimens. In both cases the curves consist of three areas: the elastic regime up to the compressive strength, the crushing regime at nearly constant plateau stress – which is referred to as crush strength – and finally the densification regime, where the cellular structure is fully compacted resulting in a steep stress increase. In case of bare compression this densification point occurs at higher compressive strains (80%) compared to stabilised compression (70%), since the cell walls are not stabilised by adhesive fillets and can be folded more densely. Loading rate has no influence on the densification point. The compressive strength is almost equal for the bare and stabilised
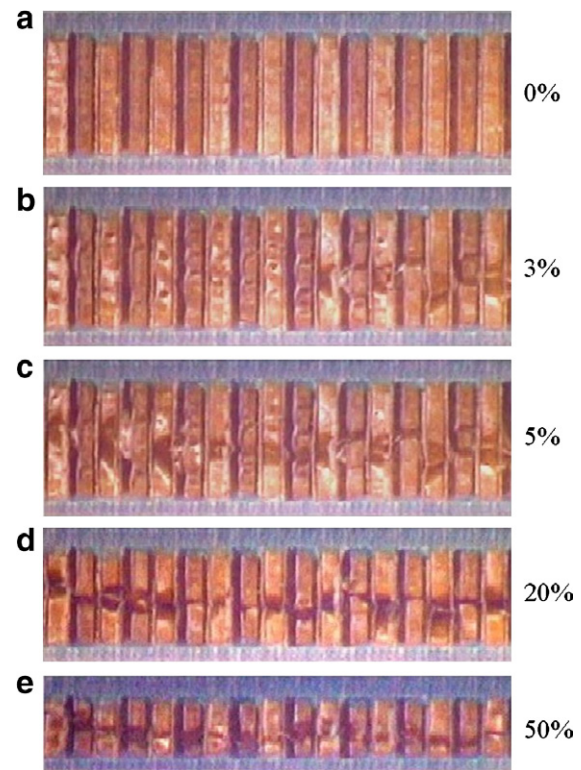

Fig. 8. Cell wall buckling deformation of stabilised hexagonal Nomex® honeycomb under compressive load in T-direction with percentage compressive strain.
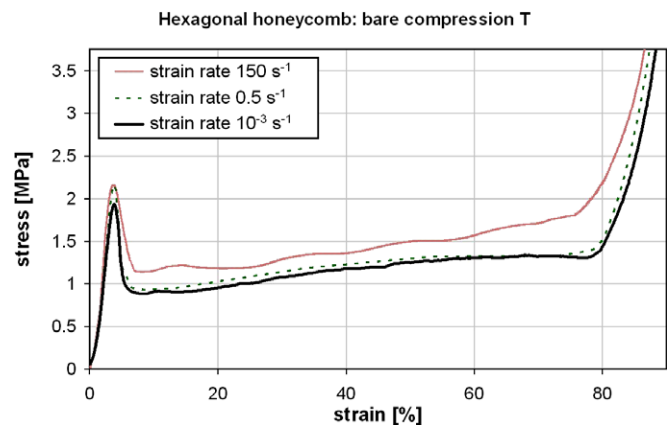

Fig. 9. Hexagonal honeycomb bare compression test results in T-direction: stress–strain-curves at different strain rates.

cases. It can be seen that dynamic loading leads to a significant increase of crush strength. In addition, the initial stiffness and compressive strength increase marginally, although the peak compressive strength is affected by the filter of the force data. This turned out to be a disadvantage of drop weight impact testing, because stress peaks cannot precisely be analysed due to data filtering as a result of oscillations. Therefore, in this investigation the increase of crush strength, i.e. the plateau stress, is primarily analysed. For the bare compression test this is about 25% at a strain rate of $150\ \mathrm{s}^{-1}$ compared to the static curve. In case
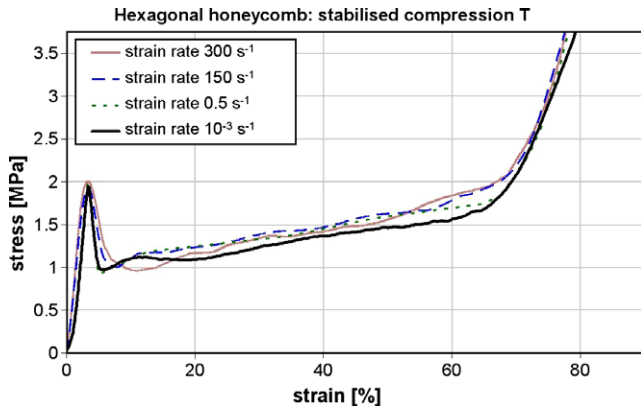
Fig. 10. Hexagonal honeycomb stabilised compression test results in T-direction: stress–strain-curves at different strain rates.

Fig. 12. Hexagonal honeycomb in-plane compression test results in W-direction: stress–strain-curves at different strain rates.

of stabilised compression, the increase is only about 10%. The explanation of this effect may be seen in the inertial response of the honeycomb structure, which will be addressed later in more detail.

The Young's modulus and plateau stress for in-plane compression behaviour are remarkably smaller than in case of flatwise compression. Expressed in terms of factors, they are 140 and 36 times smaller for the L-direction as well as 250 and 40 times smaller for the W-direction. In literature, the factor 1000 is sometimes assumed, which does not seem to be suitable in this case [40].

The in-plane compression curves exhibit the same three areas as the flatwise compression curves (Figs. 11, 12): an initial linear elastic regime, a nearly constant plateau stress, and the steep slope after compaction. However, a stress peak as in the case of flatwise compression does not occur. The shape of the curve in L-direction is rather the result of elastic cell wall bending (Fig. 13a). In the beginning the double cell walls initially oriented parallel to the loading direction remain parallel to the loading direction while the single cell walls deform elastically (linear elastic regime). This linear elastic region ends with the double cell walls folding laterally while the single cell walls are bent in
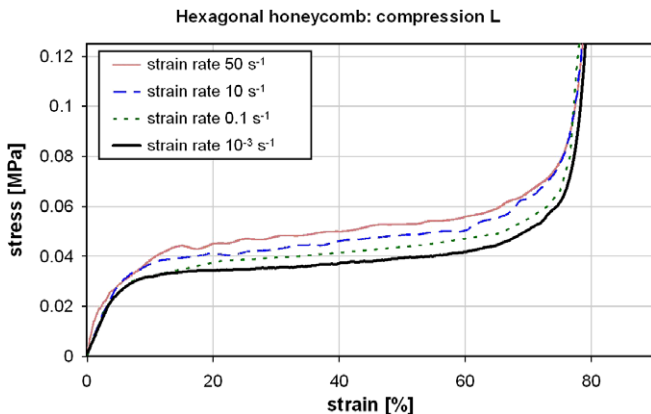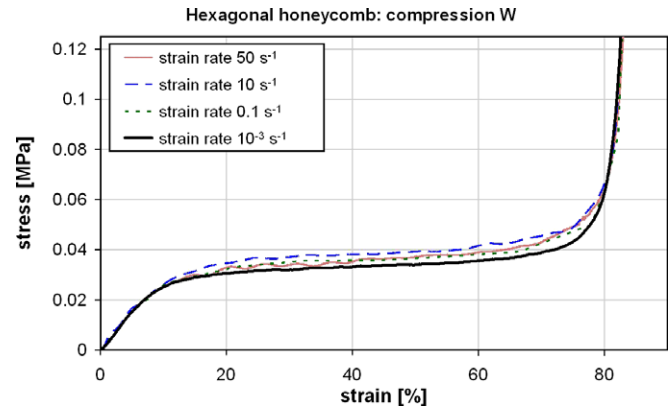
an S-shape. This folding phenomenon continues (plateau stress) until the cell walls come into contact and the cellular structure is fully compacted (steep slope). This cell wall deformation scheme occurs homogeneously throughout the whole honeycomb specimen.

In contrast to this, the deformation of cell walls in W-direction is inhomogeneous (Fig. 13b). After an initial elastic deformation of the cell walls (linear elastic regime) a local collapse of one cell wall at an arbitrary location occurs. The neighbouring cells are affected and weakened so that the whole cell row collapses while the remaining cells above and beneath keep their hexagonal shape. In the following the adjacent cell rows collapse under a constant load (plateau stress). Once all rows have collapsed the material is densified (steep slope).

For both L- and W-direction the stress–strain-curves are influenced by loading rate with a higher increase for the L-direction. Only the plateau stress level is affected while initial slope and densification point are not influenced by loading rate. The explanation for the rate dependency lies rather in the structural design of the honeycomb than in material effects. In case of the L-direction the plateau stress increases about 33% at a strain rate of $50 \, s^{-1}$ compared to the static curve. The local deformation of the cell walls is composed of a high level of bending, shifting and rotation giving inertial effects a large influence. In W-direction the increase is lower with about 10–20% because of the complete failure of single rows occurring successively one row after another and not accumulated.

4.2.2. Over-expanded honeycomb

Flatwise compression testing of over-expanded honeycomb specimens was only conducted in stabilised configuration with facesheets bonded to the honeycomb. The stress–strain-curve in Fig. 14 is of a similar shape as for the hexagonal honeycomb of same density. The stress drop after compressive strength is even more significant with a respective lower crush strength. Loading rate has a minor influence on crush strength with an increase of 10–15% for high strain rates.
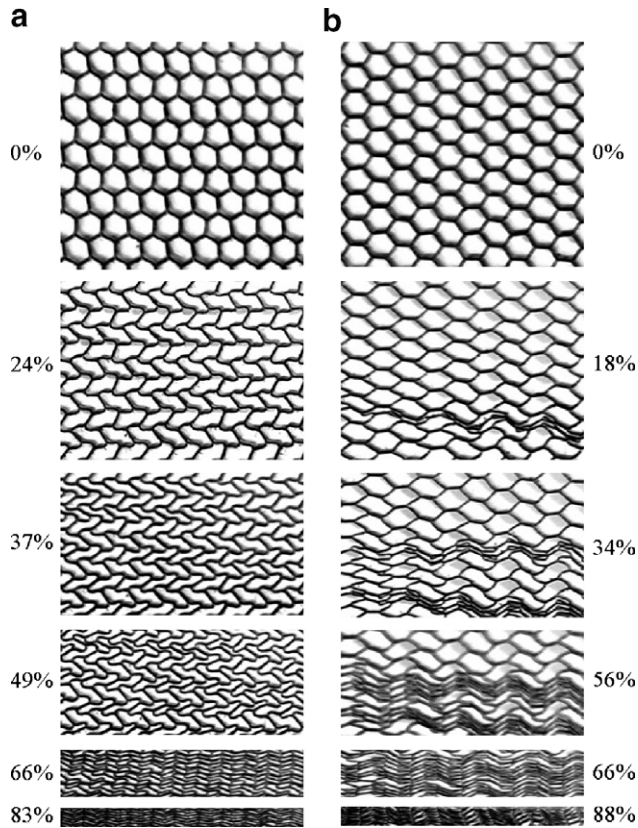

Fig. 11. Hexagonal honeycomb in-plane compression test results in L-direction: stress–strain-curves at different strain rates.

Fig. 13. In-plane cell deformation of hexagonal Nomex® honeycomb under compressive load in (a) L-direction, (b) W-direction with percentage compressive strain.
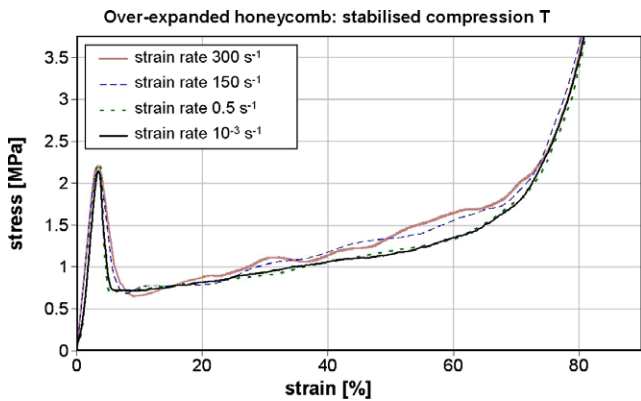

Fig. 14. Over-expanded honeycomb stabilised compression test results in T-direction: stress–strain-curves at different strain rates.
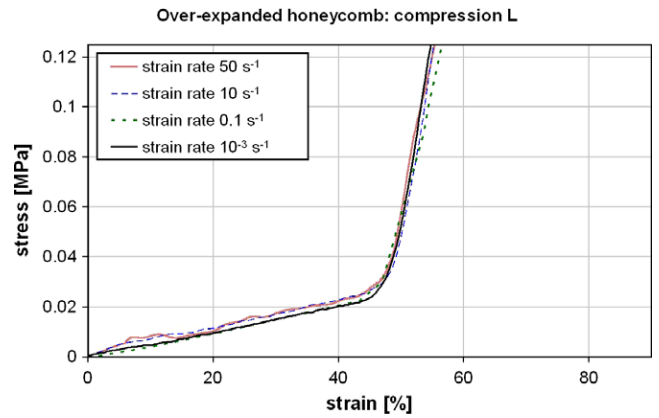

Fig. 15. Over-expanded honeycomb in-plane compression test results in L-direction: stress–strain-curves at different strain rates.

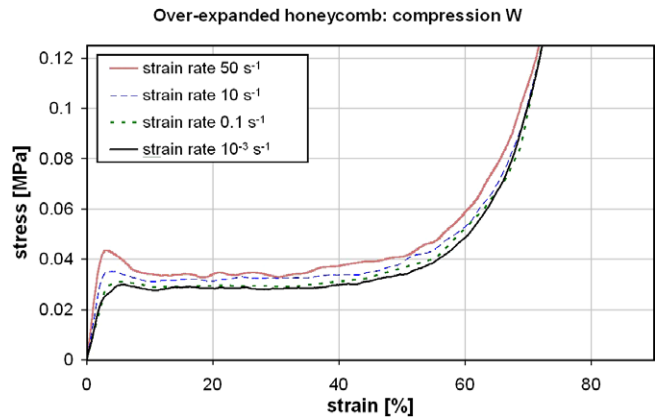Fig. 16. Over-expanded honeycomb in-plane compression test results in W-direction: stress–strain-curves at different strain rates.

The in-plane compressive stress–strain-diagram of over-expanded honeycomb specimens in L-direction (Fig. 15) differs from the diagram in W-direction (Fig. 16): There is no plateau stress but a linear elastic stress slope up to a steep increase in the strain region of about 50%. This can be explained by means of the in-plane cell deformation in Fig. 17a. The double cell walls are oriented parallel to the load direction and the load transfer occurs by elastic bending deformation of the single cell walls in an S-shape.

Here the double cell walls do not turn sideward in the following as in the case of hexagonal honeycomb, resulting in a larger linear elastic regime. In the strain region of about 50% the cells are deformed in a way that the double cell walls come into contact, which leads to the steep increase. Further compressive deformation leads to a crushing of the double cell walls. This densification point occurs much earlier than in case of the other specimens. The strain rate-affected increase of the stress-curve is about 10% at higher strain rates due to small local deformation levels at the cell walls comprising mainly of bending.

The in-plane compressive stress–strain-diagram in W-direction consists of a distinctive plateau stress as in case of hexagonal honeycomb. However, the cell deformation phenomena are completely different (Fig. 17b). Since the cell walls are continuously oriented in load direction (L-direction: discontinuously), the linear elastic slope is remarkably higher than for the hexagonal honeycomb. The result of this compressive stress state is buckling of the single cell walls at arbitrary locations. Several cells laterally buckle deforming the neighbouring cells. This initiates an irregular asymmetrical cell deformation of the specimen progressing under a constant stress level. Up to
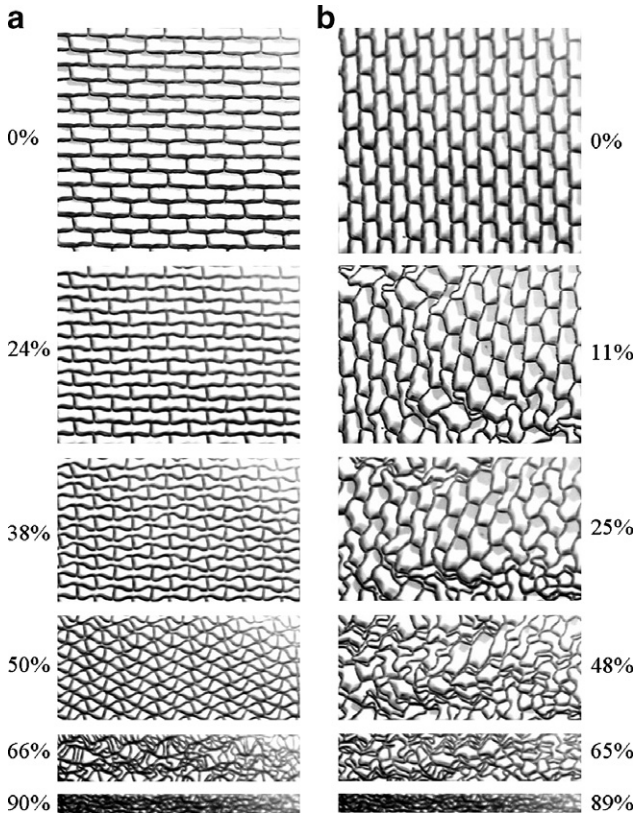
Fig. 17. In-plane cell deformation of over-expanded Nomex® honeycomb under compressive load in (a) L-direction, (b) W-direction with percentage compressive strain

a compressive strain of 48%, almost undeformed cells can still be found besides others that are highly deformed, justifying this constant stress level. In case of hexagonal honeycombs loaded in W-direction, the cell walls are ideally folded and densification occurs at strains of approximately 80% (Fig. 12). By contrast, for over-expanded specimens the cell interference occurs much earlier so that higher loads are necessary in order to further deform this irregular structure. Therefore, the stress increase begins in a strain region of 50–60% (Fig. 16). For high loading rates the formation of a stress peak following the linear elastic regime is noticeable, which is assumed to result from a higher stability of the single cell walls. The single cell walls are supported laterally by double cell walls from alternating sides. Up to a strain of about 3% this structure can bear rising loads with increasing lateral movement of the double cell walls inducing irregularities in the force transferring single cell walls at quasi-static strain rate. This leads to a stiffness reduction in stress–strain-relation and a smooth approach to the stress plateau. With higher strain rates the irregularities and the stiffness reduction are kept smaller due to inertial effects of the cell walls. As a result, the structure can bear higher loads for a small time leading to a peak stress with a sudden decrease to the stress plateau level after stability loss of the single cell walls. Even the plateau stress is affected by strain rate due to large local deformations with inertial effects and additionally due to friction

between the inhomogeneously and chaotically folding cell walls. The stress plateau increases about 23% at a strain rate of $50 \ s^{-1}$.

4.2.3. Summary

For hexagonal and over-expanded honeycomb cell configurations various crushing and collapse phenomena were observed and explained in transverse and in-plane material directions. The orientation of the double and single cell walls to the load direction has a key influence on deformation behaviour (Fig. 18). While the compressive cell deformation of hexagonal and over-expanded honeycomb in L-direction is regular and homogeneous, it is localised and inhomogeneous in W-direction. All of the stress–strain-curves turned out to be affected by loading rate. The relationship between strain rate and increase of plateau stress is illustrated in Fig. 19. Except for two contradicting data points for hexagonal honeycomb all curves are monotonically increasing towards higher strain rates. The absolute value of increase is higher for the hexagonal honeycomb than for the over-expanded honeycomb of the same density. In [20,41–43] it is depicted for aluminium honeycomb, that micro-inertial effects of the cellular structure are responsible for the strain rate increase, since the aluminium sheet material has no significant rate dependence in the respective domain and constitutive strain rate effects can therefore be ruled out. Other explanations for
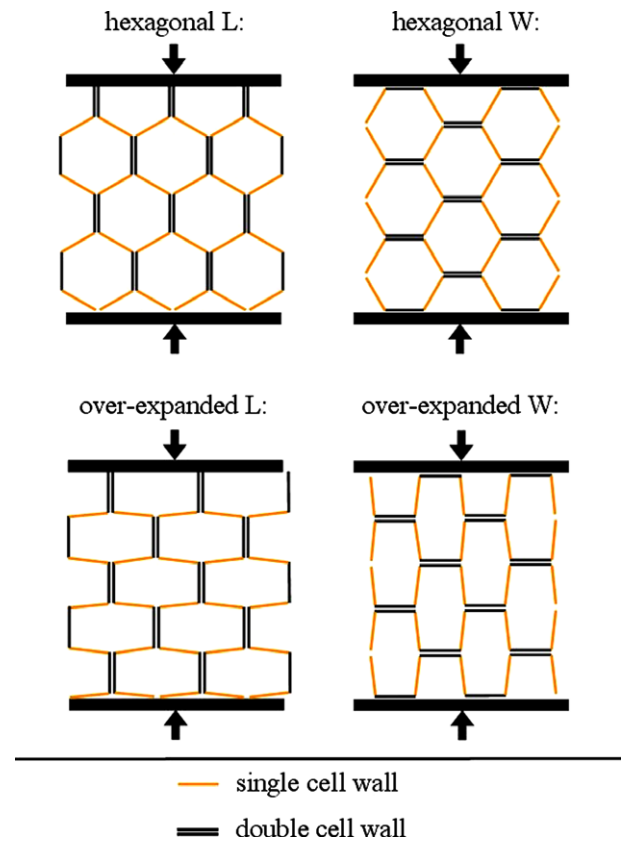

Fig. 18. Orientation of single and double cell walls to the load direction.
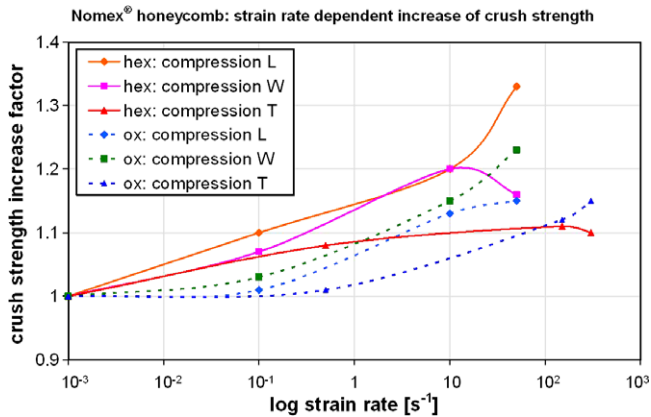
Fig. 19. Nomex® honeycomb strain rate diagram: strain rate dependent increase of plateau stress for hexagonal and over-expanded honeycomb.

the rate effect are a more complicated crushing pattern of the cells under dynamic loading as well as the influence of trapped air in case of stabilised compression [17,44,45]. However, in this experimental investigation, no trapped air effect could be observed, because in that case the stabilised compression specimens should have shown a higher rate dependency than the bare compression specimens, assuming that the air can escape from the upper and lower opening of the cells in the latter case. Quite contrary to that, the bare specimens showed a higher strain rate dependency. Therefore, the reason for the strain rate effect in this investigation is primarily ascribed to inertial effects rather than trapped air or rate effects of the cell material. This theory is supported by the fact that the stress increase is most pronounced for collapse phenomena involving large local deformations in an evenly distributed manner, where inertial effects dominate.

5. Conclusions

Dynamic testing was conducted on phenolic GFRP and phenolic-impregnated aramid paper honeycomb specimens in order to analyse the effect of loading rate on the mechanical behaviour. The strain rate effect for the composite material is remarkable and leads to increasing Young's modulus, tensile strength, tensile failure strain, shear modulus and shear strength. This strain rate effect was found to be negligible for the strain rate domain below $1\,s^{-1}$.

Also for the honeycomb specimens higher loading rates lead to an increase of the stress-curves. In this study the plateau stress was primarily analysed and compared, since the densification point was not influenced by strain rate and the peak stress could not finally be evaluated because of the strong influence of data filters. The increase of the plateau stress is about 10–30% for the honeycomb specimens in the strain rate domain from $50\,s^{-1}$ to $300\,s^{-1}$ depending on the material direction. The hexagonal cell configuration turned out to be more influenced by loading rate than the over-expanded honeycomb. The rate dependency seems to be affected more severely by the structural

design of the honeycomb than by pure Nomex® material behaviour and is ascribed to inertial effects of the buckling and folding cell walls. The data presented in this paper can be used for rate-dependent material modelling for dynamic FE-simulations of phenolic GFRP/Nomex® sandwich structures.

Acknowledgements

References

[1] Gardziella A, Pilato LA, Knop A. Phenolic resins. 2nd ed. Springer; 2000.
[2] Hunter J, Forsdyke KL. Phenolic GRP and its recent applications. Polym Compos 1989;10(2):169–85.
[3] Nyden MR, Brown JE, Lomakin SM. Flammability properties of honeycomb composites and phenol–formaldehyde resins. In Fire and polymers II: materials and tests for hazard prevention, ACS symposium series 599, Washington, DC, (USA); August 21–26th 1994. p. 245–55.
[4] Willson P. An update on phenolic resins for use in mass transport, marine, off shore and construction applications. Composites in Fire 3, Centre for Composite Materials Engineering, University of Newcastle, UK; September 9–10th 2003.
[5] Sarath Chandra D, Laramee RC. Glass/phenolic composites: properties and fracture features. In: Cheremisinoff NP, Cheremisinoff PN, editors. Handbook of advanced materials testing. Marcel Dekker, Inc.; 1995. p. 933–69.
[6] Redjel B. Mechanical properties and fracture toughness of phenolic resin. Plast Rub Compos Pro 1995;24:221–8.
[7] Charalambides MN, Williams JG. Fracture toughness characterization of phenolic resin and its composite. Polym Compos 1995;16(1): 17–28.
[8] St John NA, Brown JR. Flexural and interlaminar shear properties of glass-reinforced phenolic composites. Compos Part A 1998;29: 939–46.
[9] Morii T, Ivens J, Verpoest I. Influence of sizing and resin on the mechanical properties of unidirectional glass/phenolic composite. In: Proceedings of the 7th international conference on composite interfaces (ICCI-VII), Fujisawa, (Japan); May 10–13th 1998. p. 202–03.
[10] Morii T, Ivens J, Verpoest I. Interfacial effect on the mechanical properties of glass/phenolic composite. In: Proceedings of the 12th international conference on composite materials (ICCM-12), Paris, (France); July 5–9th 1999.
[11] Tavakoli SM, Palfrey RA, Phillips MG. Compatibility of commercial chopped-strand mats with a phenolic resin system for hand laminating. Composites 1989;20(2):159–65.
[12] Barré S, Chotard T, Benzeggagh ML. Comparative study of strain rate effects on mechanical properties of glass fibre-reinforced thermoset matrix composites. Compos Part A 1996;27:1169–81.
[13] Maji AK, Satpathi D, Donald S. Mechanical properties of aluminium honeycomb impact limiters. RAMTRANS 1992;3(2–3):109–19.
[14] Koploy MA, Taylor CS. GA-4/GA-9 Honeycomb impact limiter tests and analytical model. High Level Radioactive Waste Management. In: Proceedings of the 2nd annual international conference, Las Vegas, (NV, USA); 1991. p. 1264–70.
[15] McFarland RK. The development of metal honeycomb energy absorbing elements. JPL Report TR 32-639; July 1964.

[16] Bandak M, Bitzer T. Honeycomb, a lightweight energy absorbing material. In: 22nd international SAMPE technical conference; November 6–8th 1990. p. 1250–63.

[17] Shkolnikov MB. Honeycomb modeling for side impact moving deformable barrier. In: Proceedings of the 7th international LS-DYNA users conference, Dearborn, (MI, USA); May 20–21th 2002.

[18] Kirk JA. Mechanical energy absorbers and aluminium honeycomb. J Mech Des 1982;104:671–4.

[19] Wu E, Jiang WS. Axial crush of metallic honeycombs. Int J Impact Eng 1997;19(5–6):439–56.

[20] Zhao H, Gary G. Crushing behaviour of aluminium honeycombs under impact loading. Int J Impact Eng 1998;21(10):827–36.

[21] Baker WE, Togami TC, Weydert JC. Static and dynamic properties of high-density metal honeycombs. Int J Impact Eng 1998;21(3):149–63.

[22] Goldsmith W, Sackman JL. Energy absorption by sandwich plates: a topic in crashworthiness. Crashworthiness and occupant protection in transportation systems, ASME, vol. 126; 1991. p. 1–30.

[23] Goldsmith W, Sackman JL. An experimental study of energy absorption in impact on sandwich plates. Int J Impact Eng 1992;12(2):241–62.

[24] Aitken R. Damage due to soft body impact on composite sandwich aircraft panels. PhD Thesis, University of Auckland, Department of Mechanical Engineering; 2000.

[25] Heimbs S, Middendorf P, Maier M. Honeycomb sandwich material modeling for dynamic simulations of aircraft interior components. In: Proceedings of the 9th International LS-DYNA Users Conference, Dearborn, MI, (USA); June 4–6th 2006.

[26] Gibson LJ, Ashby MF. Cellular solids: structure and properties. 2nd ed. Cambridge University Press; 1997.

[27] Gotoh M, Yamashita M, Kawakita A. Crush behavior of honeycomb structure impacted by drop-hammer and its numerical analysis. Mater Sci Res Int 1996;2(4):261–6.

[28] Stronge WJ. Dynamic crushing of elastoplastic cellular solids. In: Jono M, Inoue T, editors. Mechanical behaviour of materials VI (ICM6), vol. 1. Oxford: Pergamon Press; 1991. p. 377–82.

[29] Hönig A, Stronge WJ. In-plane dynamic crushing of honeycomb. Int J Mech Sci 2002;44:1665–714.

[30] Papka SD. In-plane uniaxial and biaxial crushing of a polycarbonate honeycomb. PhD Thesis, University of Texas at Austin, Department of Aerospace Engineering and Engineering Mechanics; 1998.

[31] Bitzer T. Useful analysis methods for sandwich structures. In: 39th international SAMPE symposium, Anaheim, CA, (USA); April 11–14th 1994. p. 419–25.

[32] Shkolnikov MB. Strain rates in crashworthiness. In: Proceedings of the 8th International LS-DYNA users conference, Dearborn, MI, USA; 2004.

[33] Welsh LM, Harding J. Effect of strain rate on the tensile failure of woven reinforced polyester resin composites. J Phys IV 1985;46(8):C5.405–14.

[34] Yuanming X, Xing W. Constitutive equation for unidirectional composites under tensile impact. Comp Sci Tech 1996;56:155–60.

[35] Behler FJ, Wulf A. Effect of high loading rates on the mechanical properties and damage evolution of fibre reinforced plastics. In: Bunsell AR et al., editors. Developments in the science and technology of composite materials, Proceedings of the 5th European conference on composite materials, Bordeaux, France; 1992. p. 123–28.

[36] Sierakowski RL. Strain rate effects in composites. Appl Mech Rev 1997;50(12):741–61.

[37] Xia Y, Yuan J, Yang B. A statistical model and experimental study of the strain-rate dependence of the strength of fibres. Comp Sci Tech 1994;52:499–504.

[38] Rotem A, Lifshitz JM. Longitudinal strength of unidirectional fibrous composite under high rate of loading. Proceedings of the 26th annual technical conference, Society of the Plastics Industry, Reinforced Plastics/Composites Division, Washington (DC); 1971. p. 1–10 [Section 10-G].

[39] Grimes GC. The adhesive-honeycomb relationship. Appl Polym Symp 1966;3:157–90.

[40] Anderson TA. Lightweight composite structures. Department of Aeronautics and Astronautics, University of Washington; 2003.

[41] Reid SR, Reddy TY, Peng C. Dynamic compression of cellular structures and materials. In: Jones N, Wierzbicki T, editors. Structural crashworthiness and failure. Amsterdam: Elsevier; 1993. p. 295–340.

[42] Kobayashi H, Daimaruya M, Takaya Y. Dynamic and quasi-static deformation of aluminium honeycomb sandwich panel in three point bending. J Phys IV 2003;110:705–10.

[43] Harrigan JJ, Reid SR, Peng C. Inertia effects in impact energy absorbing materials and structures. Int J Impact Eng 1999;22:955–79.

[44] De Lassat de Pressigny Y. Numerical simulation of ground impact after airdrop. In: Proceedings of the 5th European LS-DYNA users conference, Birmingham, UK; May 25–26th 2005.

[45] Zhou Q, Mayer RR. Characterization of aluminium honeycomb material failure in large deformation compression, shear, and tearing. J Eng Mater-T ASME 2002;124:412–20.